Available online at www.sciencedirect.com
ScienceDirect
International Journal of Heat and Mass Transfer 50 (2007) 2434–2438
International Journal of HEAT and MASS TRANSFER
www.elsevier.com/locate/ijhmt

Technical Note

Two-dimensional numerical simulations of shock waves in micro convergent–divergent nozzles

Jinliang Xu *, Chuangxin Zhao

Micro Energy System Laboratory, Guangzhou Institute of Energy Conversion, Chinese Academy of Sciences, Nengyuan Road, Wushan, Guangzhou 510640, PR China

Received 7 April 2006; received in revised form 13 November 2006
Available online 21 February 2007

Abstract

The steady two-dimensional Navier–Stokes equations with the slip wall boundary conditions were used to simulate the supersonic flow in micro convergent–divergent nozzles. It is observed that shock waves can take place inside or outside of the micronozzles under the earth environment. For the over-expanded flows, there is a boundary layer separation point, downstream of which a wave interface separates the viscous boundary layer with back air flow and the inviscid core flow. The oblique shock wave is followed by the bow shock and shock diamond. The viscous boundary layer thickness relative to the whole nozzle width on the exit plane is increased but attains the maximum value around of 0.5 and oscillates against this value with the continuous increasing of the nozzle upstream pressures. The viscous effect either changes the normal shock waves outside of the nozzle for the inviscid flow to the oblique shock waves inside the nozzle, or transfers the expansion jet flow without shock waves for the inviscid flow to the oblique shock waves outside of the nozzle.

Keywords: Shock wave; Micronozzle; Viscous effect; Microthruster

1. Introduction

Macroscale convergent–divergent nozzles can convert the upstream static pressure and thermal energy into the kinetic energy to create supersonic flow. Shock wave may take place with the flow expansion into the atmospheric pressure environment [1]. The fast development of MEMS fabrication technology leads to the development of micronozzles, which were reported to be used in microthruster system for the attitude control of the micro/nanosatellites [2]. Even though the shock wave does not exist due to the lack of the background pressure with the micronozzle operating in the space environment, it may occur when the micronozzle is tested in the laboratory environment where the background pressure is around 1 bar. The newly proposed microturbine system can either provide the electricity output, or can be used as a microrocket [3]. For the later application, the hot gas at the microcombustor exit is discharged through a micronozzle.

Bayt [2] performed the modeling, design and testing of micron scale convergent–divergent nozzles. The flow in the nozzle is modeled by a two-dimensional finite volume Navier–Stokes simulation. Thomas et al. [4] reported effects of inlet geometry on the mixing and performance of microthrusters. Helium, nitrogen and carbon dioxide were the tested gases. The specific impulse, thrust coefficient and characteristic velocity are found to be very different from those values predicted for the regular sized nozzles due to the viscous effects and the thick boundary layer. Alexeenko et al. [5] performed both the Direct Simulation Monte Carlo (DSMC) and the continuum flow modeling for the silicon micronozzles. Thrust losses occur because the shear on the wall is greater in a flat nozzle configuration than that in an axisymmetric conical nozzle. Kujawa and Hitt [6] reported the transient shutdown simulations of a MEMS supersonic nozzle. Under the steady state the viscous boundary layer occupies nearly half of

* Corresponding author. Tel./fax: +86 20 87057656.
E-mail address: xujl@ms.giec.ac.cn (J. Xu).

0017-9310/$ - see front matter © 2007 Elsevier Ltd. All rights reserved.
doi:10.1016/j.ijheatmasstransfer.2006.11.036

Nomenclature

a	sonic velocity (m/s)
C_p	specific heat of air at constant pressure (J/kg K)
C_v	specific heat of air at constant volume (J/kg K)
k	thermal conductivity of air (W/m K)
Kn	Knudsen number
L_1	length of the nozzle converging section (m)
L_2	length of the nozzle diverging section (m)
m	air mass flow rate (kg/s)
m_{backin}	air mass flow rate from the environment to the nozzle in the viscous boundary layer on the nozzle exit plane (kg/s)
m_{backout}	air out mass flow rate in the viscous boundary layer on the nozzle exit plane (kg/s)
m_{in}	air mass flow rate at the entrance cross section of the nozzle (kg/s)
m_{out}	air out mass flow rate in the inviscid core flow region on the nozzle exit plane (kg/s)
Ma	Mach number
p	pressure (Pa)
Pr	Prandtl number
R	air gas constant (J/kg K)
Re	Reynolds number
S	half width of the nozzle exit plane (m)
$S1$	width of the viscous boundary layer with back flow on the nozzle exit plane (m)
$S2$	half width of the inviscid core flow on the nozzle exit plane (m)
T	temperature (K)
u	velocity component in x coordinate (m/s)
v	velocity component in y coordinate (m/s)
w	width of the planar micronozzle (m)
x	axial flow coordinate (m)
y	perpendicular coordinate (m)
δ_{nozzle}	depth of the planar micronozzle (m)
γ	specific heat ratio, equals to C_p/C_v
μ	air viscosity (kg/m s)
ρ	air density (kg/m^3)
θ	half diverging angle (°)
σ_v	the tangential-momentum-accommodation coefficient
σ_T	the temperature-accommodation coefficient
ΔT	temperature difference between the gas and the entrance reference value (K)

Subscripts

gas	gas state
o	nozzle entrance condition
wall	parameters on the wall surface

the nozzle cross section on the nozzle exit plane. During the valve closure the viscous boundary layer expands to fill the entire exit plane and severely chokes the flow.

The literature survey shows that there are no studies on the shock waves in micronozzles. In the present paper the shock waves are investigated by the steady two-dimensional Navier–Stokes equations with the slip wall boundary conditions. The shock wave flow structure in micronozzles is described and the effect of the viscous effect on the shock waves is discussed.

2. Numerical simulation of the micro convergent–divergent nozzle

2.1. Description of the micronozzle geometry and grid generation

The two-dimensional micronozzles are characterized by the converging length of L_1, the throat width of w, the half diverging angle of θ, and the diverging length of L_2. In the present paper, $L_1 = 0.0005$ m but L_2 and θ are varied from 1.0 mm to 3.0 mm and 5° to 15° respectively. The whole computational domain consists of the micronozzle itself and the far field area, which is selected as 0.05 m by 0.03 m. A non-uniform grid system was shown in Fig. 1 for $L_2 = 1.0$ mm and $\theta = 15°$. The working fluid is air and the backpressure of the nozzle is 1.013 bar.

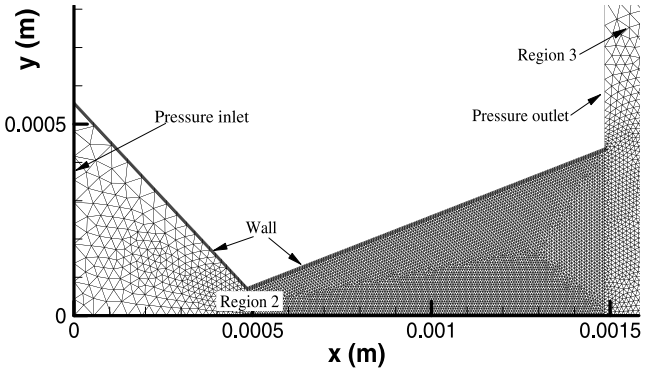

Fig. 1. Grid generation for the micronozzle with the diverging length of 1.0 mm and the half diverging angle of 15°.

2.2. The governing equations and boundary conditions

The governing equations consist of one mass, two momentum and one energy conservation equations [1], coupled with an ideal gas state equation $p = \rho RT$. It is noted that the viscous dissipation term in the energy equation should be included, which is written as

$$\varphi = 2\mu\left[\left(\frac{\partial u}{\partial x}\right)^2 + \left(\frac{\partial v}{\partial y}\right)^2 + \frac{1}{2}\left(\frac{\partial v}{\partial x} + \frac{\partial u}{\partial y}\right)^2 - \frac{1}{3}\left(\frac{\partial u}{\partial x} + \frac{\partial v}{\partial y}\right)^2\right]. \quad (1)$$

The mass flow rate is written as

$$m = \int_{-w(x)/2}^{w(x)/2} \rho u \delta_{\text{nozzle}}\, \mathrm{d}y = \rho_{\text{o}} u_{\text{o}} \delta_{\text{nozzle}} w_{\text{o}}. \quad (2)$$

The temperature dependent air viscosities and thermal conductivities are cited from Shi et al. [7] and written as $\mu = \mu_{\text{o}}(T/T_{\text{o}})^{0.76}$ and $k = k_{\text{o}}(T/T_{\text{o}})^{0.86}$, which are valid over the temperatures from room to 1000 K with the maximum relative error less than 6%.

Gas flow in MEMS devices has not been well understood yet. Gad-el-Hak [8] recommends the Knudsen number to characterize the microscale gas flow, which is written as

$$Kn = \sqrt{\frac{\pi\gamma}{2}}\frac{Ma}{Re}. \quad (3)$$

The local Ma number is computed as $Ma = \sqrt{u^2 + v^2}/a$. The Re number is defined as $Re = \rho \int_{-w(x)/2}^{w(x)/2} u\,\mathrm{d}y/\mu$. The continuum flow model with the slip wall boundary condition is valid if $10^{-3} < Kn < 10^{-1}$, while the continuum flow model without the slip wall boundary condition is valid as long as $Kn < 10^{-3}$. Because the side wall surface of the nozzle is inclined, the first order slip velocity on the wall surface is written regarding the parameter gradients along the wall surface "s" and perpendicular to the wall surface "n", based on [8]:

$$u_{\text{gas}} - u_{\text{wall}} = \frac{2-\sigma_v}{\sigma_v} Kn \left(\frac{\partial u}{\partial n}\right)_w + \frac{3}{4}\frac{\Delta T}{T_0}\frac{1}{Re}\left(\frac{\partial T}{\partial s}\right)_w, \quad (4)$$

$\sigma_v = 1$ states that significant slip occurs only if the mean velocity of the molecules varies appreciably over a distance of one mean free path [8]. The temperature jump at the wall surface is computed as

$$T_{\text{gas}} - T_{\text{wall}} = \frac{2-\sigma_T}{\sigma_T}\left[\frac{2\gamma}{\gamma+1}\right]\frac{Kn}{Pr}\left(\frac{\partial T}{\partial n}\right)_w. \quad (5)$$

2.3. Running the code

Because the shock waves are encountered in the present study, a denser grid generation is needed across the shock wave interfaces. The slip wall boundary conditions are fulfilled by a User Defined Function (UDF). The two-dimensional steady Navier–Stokes equations are solved using the coupled explicit solver within the FLUENT 6.1 software package. Initially the first-order upwind scheme is applied to accelerate convergence. Upon the first-order convergence, the second-order discretization schemes are implemented until the complete solution convergence. The variables residuals and flow monitors established at key locations within the computational domain are examined. The conservation of the mass flow rate is monitored over the entire domain together with simultaneous monitoring of the value at the nozzle throat to the exit plane to verify the complete convergence of the solution.

The two-dimensional model can be used to describe the flow in a nozzle of a flat geometric configuration if the influence of the end walls is neglected. Most of available numerical simulations on micronozzle flow without shock waves are two-dimensional ones [2,7,9]. Recently, Zhang et al. [10] performed the comparisons between two and three-dimensional simulations and found that the supersonic flow in micronozzles can be modeled by the two-dimensional theory if the etched nozzle depth is more than ten times of the throat width. The three-dimensional effect becomes more apparent with decreasing the nozzle depth to the throat width ratio. This is because the entire nozzle exit is affected by the wall boundary layer, with greater impact of the viscous effect on the nozzle performance [5]. Under such condition the three-dimensional flow modeling is required to predict accurately the nozzle performance.

3. Results and discussion

Fig. 2 shows the streamline of the flow field and the Mach number contours over the computational domain at the nozzle upstream pressure of 6.4 bar. The shock wave flow structure has the following characteristics: (a) There is a boundary layer separation point downstream of the throat. (b) There is a wave interface separating the viscous boundary layer with back flow and the inviscid core flow. The velocities are very small along the formed wave interface, with positive x flow inside the inviscid core flow and negative x flow in the viscous boundary layer region.

As shown in Fig. 2b, the Mach number is around 0.8 at the throat for the supersonic flow in the diverging section. The unity Mach number is not exactly at the throat location, but a little bit downstream of the throat. This phenomenon is similar to that was predicted by Bayt [2]. The primary effect will be a reduction in the effective area ratio due to blockage from the viscous boundary layer. This effect causes the effective minimum cross section is not at the throat location but a little bit downstream of the throat and the unity Mach number occurs there. Downstream of the throat a successive conical shape Mach number rings are observed. These Mach number rings are enveloped with each other, with larger Mach numbers inside the smaller conical shape Mach number ring, until a very tiny conical shape Mach number ring appears, inside which the maximum Mach number throughout is populated. The smallest conical shape Mach number ring, with the maximum Mach number identified as 2.7 is observed with the tip points of the smallest conical shape Mach number ring located at $x = 1.567$ mm.

The smallest conical shape Mach number ring is well consistent with a pair of oblique shock waves, perpendicular to the two inclined surfaces of the Mach number ring. The bow shock and shock diamond are followed by the oblique shock waves.

Fig. 3 illustrates the flow field near the nozzle exit plane. Two vortices are observed, with one in the viscous boundary layer inside the nozzle diverging section, the other near the upper corner of the nozzle. Again the flow field is

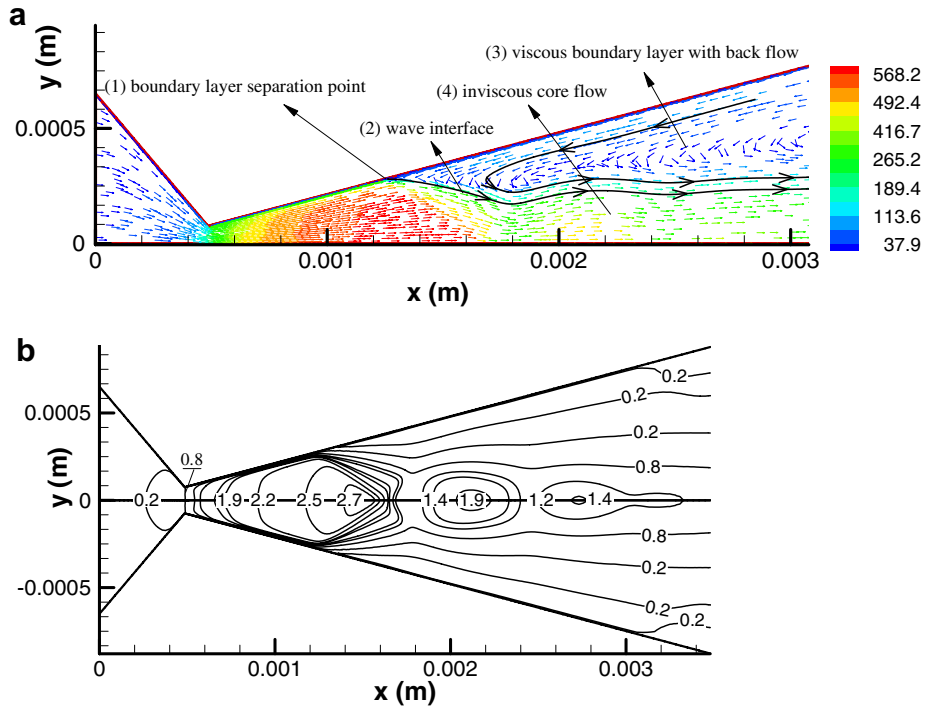

Fig. 2. The streamline of the flow field and the Mach number contours for $L_1 = 0.5$ mm, $L_2 = 3.0$ mm and $\theta = 15^\circ$ at $p_o = 6.4$ bar.

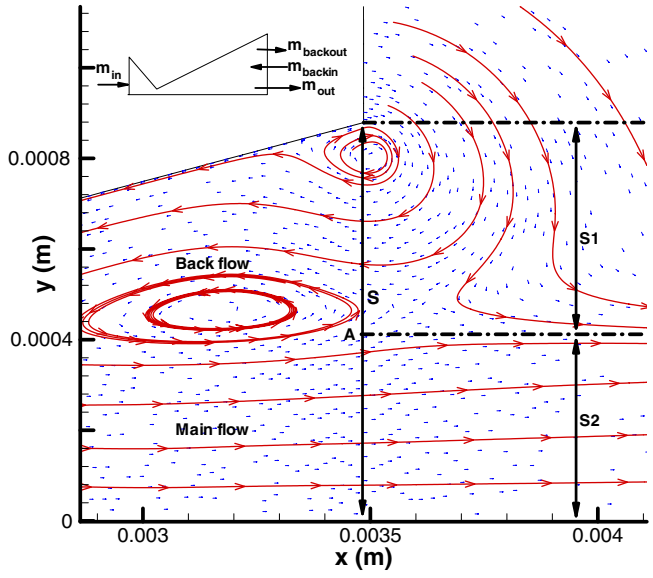

Fig. 3. Back flow phenomenon near the micronozzle exit plane at the upstream pressure of 6.4 bar.

divided into the viscous boundary layer with back flow and the inviscid core flow. We consider the balance of the mass flow rate of the air on the exit plane. We record the back air flow rate as m_{backin}, and the out flow rate as m_{backout} in the viscous boundary layer. Meanwhile, we record the out flow rate as m_{out} in the inviscid core flow on the nozzle exit plane. Assuming the net air flow rate as m_{in} ($m_{\text{in}} = m$), the mass conservation principle yields the following expression for the above mentioned air flow rates

$$m_{\text{in}} = \underbrace{m_{\text{out}}}_{\text{inviscid core flow region}} + \underbrace{m_{\text{backout}} - m_{\text{backin}}}_{\text{viscous boundary layer region}}. \quad (6)$$

In Fig. 3, S indicates the half width of the nozzle exit plane, with $S1$ and $S2$ representing the half width of the viscous boundary layer and the inviscid core flow regions respectively. It is observed that $S2/S$ and $S1/S$ do not change significantly at higher upstream pressures, and may oscillate around the value of 0.5, indicating that the viscous boundary layer is very thick and may cover half of the nozzle width on the exit plane.

Viscous effect is important to affect shock waves in microscale due to the large surface to volume ratio. Fig. 4 illustrates the detailed comparisons of the viscous and inviscid micronozzle flow with $\theta = 5^\circ$ and $L_2 = 3.0$ mm at $p_o = 6.4$ bar. The inviscid nozzle flow was modeled by setting the air viscosity to be zero manually. As shown in Fig. 4a, the normal shock wave occurs near the nozzle exit plane with the oblique shock waves near the two corner regions of the nozzle exit plane. The pressure difference from the supersonic flow to the ambient atmosphere is adjusted by the shock wave. However, the viscous effect leads to the complicated oblique shock wave flow structure (see Fig. 4b). A separation point appears to separate the viscous boundary layer with back flow from the ambient and the inviscid core flow. Downstream of the separation point, the oblique shock wave exists followed by the bow shock and shock diamond. The low static pressure before the lip of the oblique shock wave leads to rapid compression and deceleration of the gas flow as the gas penetrates into the oblique and bow shocks, and the high

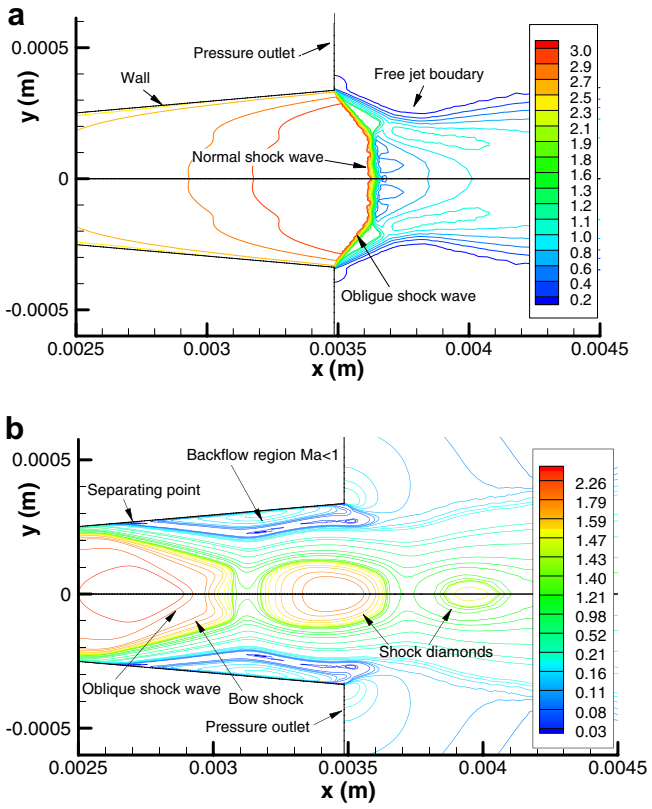

Fig. 4. Mach number contours by viscous and inviscid theory (a and b: $L_2 = 3.0$ mm, $\theta = 5^\circ$, $p_o = 6.4$ bar, (a) for inviscid flow and (b) for viscous flow).

static pressure after the oblique and bow shocks leads to rapid expansion and acceleration till the shock diamonds occur. In either case, if the inviscid flow theory predicts the expansion jet flow without shock waves, the viscous effect then yields the oblique shock waves outside of the micronozzle.

4. Conclusions

In this paper we presented the two-dimensional Navier–Stokes equations with the slip wall boundary conditions to simulate the supersonic flow with the shock wave flow structure in the micro convergent–divergent nozzles. The working fluid is air and the fluid is discharging into the atmospheric pressure environment. A separation point is observed on the nozzle wall surface. Downstream of the separation point a wave interface separates the viscous boundary layer and the inviscid core flow. The oblique shock wave is found to be followed by the bow shock and shock diamond. At the nozzle exit plane the viscous boundary layer may cover half of the whole nozzle exit width. The viscous effect in microscale is important to form the shock wave flow structure in the micronozzles.

Acknowledgements

This work is supported by the international cooperation project funded by Chinese Academy of Science (GJHZ05), the Natural Science Foundation of Guangdong Province (5000729) and the National Natural Science Foundation of China (50476088).

References

[1] M.C. Poter, D.C. Wiggert, Mechanics of Fluids, second ed., London, 1997.
[2] R.L. Bayt, Analysis, fabrication and testing of a MEMS based micropropulsion system, PhD Thesis, Department of Dynamics and Aeronautics, Massachusetts Institute of Technology, Cambridge, MA 02139, USA, 1999.
[3] A.H. Epstein, S.D. Senturia, I.A. Waitz, Microturbomachinery, US Patent, Patent No. 5932940, 1999.
[4] R. Thomas, B. Baird, A.R. Choudhri, S.R. Gollahalli, Effects of inlet geometry on the mixing and performance of microthrusters, 40th AIAA Aerospace Sciences Meeting and Exhibit, Reno, NV, January 2002, AIAA Paper 2002-1030.
[5] A.A. Alexeenko, D.A. Levin, S.F. Gimelshein, R.J. Collins, B.D. Reed, Numerical modeling of axisymmetric and three-dimensional flows in microelectromechanical systems nozzles, AIAA J. 40 (5) (2002) 897–904.
[6] J. Kujawa, D.L. Hitt, Transient shutdown simulation of a realistic MEMS supersonic nozzle, 40th AIAA/ASME/SAE/ASEE Joint Propulsion Conference and Exhibit, Ft. Lauderdale, FL, July 2004, AIAA Paper 2004-3762.
[7] W. Shi, M. Miyamoto, Y. Katoh, J. Kurima, Choked flow of low density gas in a narrow parallel-plate channel with adiabatic walls, Int. J. Heat Mass Transfer 44 (2001) 2555–2565.
[8] Gad-el-Hak, The fluid mechanics of microdevices—the Freeman scholar lecture, ASME J. Fluid. Eng. 121 (5) (1999) 5–33.
[9] W.F. Louisos, D.L. Hitt, Optimal expansion angle for viscous supersonic flow in a 2-D micro-nozzles, 35th AIAA Fluid Dynamics Conference and Exhibit, Toronto, Ontario Canada, June 2005, AIAA Paper 2005-5032.
[10] G.X. Zhang, X.D. Cai, M.H. Liu, Y.L. Chen, Cold flow field and propulsive performance of a micro Laval nozzle, J. Propul. Technol. 25 (1) (2004) 54–57 (in Chinese).